Chemical Physics Letters 683 (2017) 216–221

Contents lists available at ScienceDirect

Chemical Physics Letters

journal homepage: www.elsevier.com/locate/cplett

Research paper

Quantum controlled fusion

Eduardo Berrios [a], Martin Gruebele [b,*], Peter G. Wolynes [c,*]

[a] Facultad de Ciencias Químicas y Farmacéuticas, Universidad de Chile, Santos Dumont N° 964, Independencia, Chile
[b] Departments of Chemistry and Physics, University of Illinois at Urbana–Champaign, 600 S. Mathews Ave., Urbana, IL 61801, USA
[c] Departments of Chemistry and Physics, Rice University, 6100 Main Street, Houston, TX 77251, USA

ARTICLE INFO

Article history:
Received 2 January 2017
In final form 13 February 2017
Available online 16 February 2017

Keywords:
Quantum control
Boron hydride
Tritium
Deuterium
Feit-Fleck algorithm

ABSTRACT

Quantum-controlled motion of nuclei, starting from the nanometer-size ground state of a molecule, can potentially overcome some of the difficulties of thermonuclear fusion by compression of a fuel pellet or in a bulk plasma. Coherent laser control can manipulate nuclear motion precisely, achieving large phase space densities for the colliding nuclei. We combine quantum wavepacket propagation of D and T nuclei in a field-bound molecule with coherent control by a shaped laser pulse to demonstrate enhancement of nuclear collision rates. Atom-smashers powered by coherent control may become laboratory sources of particle bursts, and even assist muonic fusion.

1. Introduction

Nuclear reactions involving the close approach of charged particles have much smaller cross sections than do chemical reactions at ambient thermal energy. Obtaining reasonable reaction rates for nuclear fusion by thermal means thus requires achieving simultaneously high densities and temperatures. Such extreme conditions are difficult to control in thermal plasmas [1], laser-compressed fuel pellets [2], or within small clusters of ordinary molecules subject to intense laser excitation [3,4]. Even in a molecular cluster, much of the absorbed laser energy is thermalized through intracluster collisions. As a result, the cluster is blown apart, decreasing fusion yields. A novel approach to circumvent the confinement problem in thermal plasmas has been suggested: a solid state plasma confined by the quantum pinch effect in a semiconducting wire [5].

Fusion reactions also can be induced by non-thermal means. For example, charged particle beams can be collided at appropriately high energy to carry out fusion reactions in the laboratory [6]. Alternatively, fusion can be catalyzed by achieving a high spatial density, as happens for the nuclei within a muonic molecule. When a muon replaces the electron, it brings the nuclei ~200 times closer together than in an ordinary molecule, greatly enhancing the spontaneous nuclear reaction rate even at low temperature [7]. In many ways, the ground state of such a molecule is the ideal situation for fusion because the phase space density of the reacting species takes on the largest possible value consistent with quantum mechanics. While greeted by much excitement when it was discovered in the 1950s, muon-catalyzed fusion still just falls a bit short of practicality because of the insufficient lifetime of the muon.

Fusion does not occur to a measurable extent in the ground state of normal molecules bound by electrons because of the lower density of nuclei (~1/Å^3, not 1/pm^3) and the low vibrational energy (meV, not keV) compared to muonic molecules. In this paper we will explore whether laser pulse shaping could allow quantum control to enhance intramolecular nuclear collision rates, starting from normal internuclear distances. We begin with a field-bound DT^+ molecule, whose electron has been stripped away by strong-field or VUV ionization [8]. Purely field-bound molecules have already been proposed as a route to nuclear fusion [9], and have been simulated classically [10]. Following rapid ionization, the nuclei would already be at an ordinary chemical bond distance of about ~2 a.u. (~1.06 Å). While this falls short of the density in muonic molecules, it nonetheless greatly improves upon nuclear densities in plasmas. A controlled, properly shaped laser pulse could then coherently interact with the two nuclei to guide them together at sufficiently high energy so as to enhance fusion in the laboratory.

In other words, in this letter we ask, "Can a single molecule controlled by a laser pulse be turned into a nuclear accelerator?" We will explore this question computationally, using fully quantum-mechanical wavepacket propagation of the nuclear wavepacket. The goal here is to find the time dependence of a strong

* Corresponding authors.
E-mail addresses: mgruebel@illinois.edu (M. Gruebele), pwolynes@rice.edu (P.G. Wolynes).

http://dx.doi.org/10.1016/j.cplett.2017.02.045
0009-2614/

electromagnetic field optimally chosen to focus the nuclear wavepacket of a molecule to a small transverse cross section, while also dramatically increasing the center of mass collision energy. To carry out such a calculation with complete realism is demanding computationally. In our study therefore we will examine the dynamics on a two-dimensional computational grid limited to momenta corresponding to roughly 13.9 keV of relative nuclear kinetic energy, while the DT cross section peaks at roughly 65 keV (center-of-mass frame) [11]. Nevertheless, the calculations show that increased localization of the nuclear wavefunction within a $1.9 \cdot 10^{-3}$ a.u. ($\sim$0.001 Å) distance (*vs.* the original bond distance of *ca.* 2 a.u.) can be achieved by an optimized control field, thus potentially increasing nuclear reaction rates up to 16 orders of magnitude. Although we focus on the example of conventional D + T fusion, the same principles elucidated here should apply to other fusion reactions. For example, B + H aneutronic fusion [12] requires even higher center-of-mass collision energy than D + T, but it has the advantage of producing just three α-particles and a γ-ray. We will discuss the difficulties in achieving higher energies both computationally and in the laboratory, in our conclusions.

2. Computational approach

2.1. General considerations

Wavepacket calculations will be carried out for a two-dimensional (2-D) cartesian toy model with one longitudinal (along the internuclear axis) and one transverse electromagnetic field polarization. The D + T reaction has a maximum fusion cross-section of approximately $5 \cdot 10^{-24}$ cm^2 at 65 keV [11]. The corresponding $2 \cdot 10^{-4}$ Å target size in 2-D results in an angular ratio of $0.53/2 \cdot 10^{-4} \approx 3000$. Quantum theory suggests that this is the minimum number of photons required by angular momentum conservation to be absorbed, so as to form a fully focused wavepacket by multi-photon absorption. (The angular momentum of each photon is 1 $\hbar$.) To achieve 65 keV of relative center of mass motion, roughly 22 eV of energy per photon would be required to achieve full focusing with the minimum number of photons. We will instead calculate the optimum field for 1.5 eV photons ($\lambda \approx 800$ nm) that are readily available from modern regenerative amplifiers at high power. The corresponding computational grid is ten times coarser than the one that would be needed to reach the peak fusion cross section. Even this goal, modest compared to maximum confinement, showcases the possibility of quantum control of nuclear processes. In 3-D, a second control field is required, propagating perpendicular to the original 2-D control field. This addition introduces a second transverse polarization direction, which would be required to achieve a similar degree of control as in 2-D.

In our toy model, designed to highlight nuclear coherent control, we neglect the dynamics of the electron originally present in the DT^+ molecule, since it can be removed by an appropriate pre-pulse [10]. In any event, our present goal is not to find the exact shape of the optimal pulse. Finding a practically optimal pulse likely will require direct optimization of the pulse shape with laboratory experiments because of the difficulty of achieving an exact numerical solution of the multi-particle Schrödinger equation. Instead we intend to show with our toy model what enhancements in nuclear localization are plausible by adding coherent control to the intense laser pulse that forces together the nuclei after the pre-pulse.

Ignoring the electron may create additional difficulties in practice. First, the control field will unavoidably accelerate the electrons after ionization, which therefore will radiate some of the input power away. In a classical thermonuclear reactor, analogous radiation losses from Bremsstrahlung are a major constraint on operations [13]. As an order of magnitude estimate of this effect, consider a DT^+ molecular ion beam subjected to a 5 fs field ionization pulse to make DT^{2+}. The pre-pulse is then followed by a 5 fs control pulse. Both pulses can be achieved easily in the laboratory with 1.5 eV photons. At a minimum, one electron per molecule needs to be moved outside the range of a diffraction-limited $\lambda = 800$ nm ($d = 400$ nm) control beam, with an acceleration $a \approx 2 \cdot 400 \cdot 10^{-9}\ \mathrm{m}/(5 \cdot 10^{-15}\ \mathrm{s})^2$, so that Bremsstrahlung is no longer an issue. The Bremsstrahlung radiated during this process is approximately [14]

$$P(\mathrm{W}) \cdot \Delta t = \frac{\mu_0 q^2 a^2 \gamma^6 \Delta t}{6\pi c} \approx \frac{4\pi 10^{-7} (1.6 \cdot 10^{-19})^2 (1.6 \cdot 10^{21})^2 1^6 5 \cdot 10^{-15}}{6\pi 3 \cdot 10^8}\mathrm{J} \approx 3 \cdot 10^{-23}\mathrm{J} \approx 0.2\,\mathrm{meV} \quad (1)$$

In Eq. (1), μ_0 is the permittivity of free space, q the elementary charge, γ the Lorentz factor, Δt the pulse duration, and c the speed of light. For exothermicities on the order of 10 MeV (D − T or B − H fusion), 0.2 meV is negligible unless the fraction of successful fusions events per pulse drops below $\approx 10^{-10}$.

Secondly, the light electrons will be accelerated far from the nuclei (400 nm in the above example). If we treat the electrons by a classical mean field, the influence of the electrons would effectively vanish if they were ejected from the molecule in a spherically symmetrical s-wave. Even in the worst-case scenario of highly directional electron ejection, the ratio of nuclear to electronic Coulomb interaction is about (0.1 nm/400 nm) $\approx$ 0.000025, resulting in a correspondingly small correction to the effective internuclear repulsion. Such fluctuations in the electron motion may, however, lead to uncontrollable defocusing of the nuclear wavepacket.

Full electron-nuclear recollisions, which could not be treated by a mean field, can be circumvented on the <10 fs time scale of the controlled fusion event. Recollisions are desirable in high harmonic generation. They require high-Z nuclei (Ne or Ar) as well as special 'DOG' circular polarization sequences to get the electron back to the nuclei after field ionization [15]. This suggests that it should be possible to design "anti-re-collision" ionization pulses, by using linearly polarized light instead of counter-circularly polarized light for the ionization process, at least for the low-Z nuclei, such as D, T, H and B, which are the most interesting from the point of view of nuclear fusion.

The propagation of the nuclear wavepacket is carried out fully quantum mechanically using a numerical split-operator method [16]. The resulting control problem seeks to maximize the nuclear fusion yield, while constraining the laser field to be no stronger than what can be easily achieved today by focussing an amplified 800 nm laser. Our simulations solve numerically the non-relativistic time-dependent Schrödinger equation in 2-D for our toy model of two nuclei with charges q_1 and q_2 and masses m_1 and m_2 separated by a distance R. We assume zero angular momentum for the initial state, justified for a diatomic molecule ground state. Although not a complete 3-D solution, this set-up models dispersion of the wavepacket transverse to the internuclear axis, thus incorporating the major difficulty of focusing a nuclear wavepacket with a coherent control laser pulse.

We use the dipole approximation, which should be valid as long as the dimensions of the molecule do not approach the wavelength of the near-infrared photons used to control fusion. For higher frequency lasers, the interaction with the molecule would have to be treated through a vector potential with the spatial dependence included.

2.2. Numerical treatment

The Cartesian 2-D Hamiltonian in the center of mass frame can be written as:

$$H_{rel} = \frac{p^2}{2\mu} - \frac{q\boldsymbol{p}\cdot\boldsymbol{A}}{c\mu} + \frac{q_1 q_2}{R} + \frac{A^2}{2c^2}\left(\frac{q_1^2}{m_1} + \frac{q_2^2}{m_2}\right). \tag{2}$$

$\boldsymbol{A}$ is the vector potential of the laser field, $\mu = m_1 m_2/(m_1 + m_2)$ is the reduced mass, $q = \mu(q_1/m_1 - q_2/m_2)$ is the effective charge, and c is the velocity of light. In the dipole approximation the vector potential is space independent, so the last term in Eq. (1) only gives a time-dependent phase, which can be left out of the optimization. Therefore, the Schrödinger equation to be solved in atomic units (a.u.) is given by:

$$i\frac{\partial\varphi(x,y,t)}{\partial t} = \left(-\frac{1}{2\mu}\left(\frac{\partial^2}{\partial x^2} + \frac{\partial^2}{\partial y^2}\right) + \frac{iq}{c\mu}\left(A_x(t)\frac{\partial}{\partial x} + A_y(t)\frac{\partial}{\partial y}\right) + \frac{q_1 q_2}{R}\right)\varphi(x,y,t) \tag{3}$$

This equation is propagated in time by employing a second-order split operator method in the Fourier basis. The propagator is defined as [16]:

$$e^{-iH(x,y,t)\Delta t} = e^{-i\Delta tV/2}e^{-i\Delta tT}e^{-i\Delta tV/2} + O(\Delta t^3), \tag{4}$$

where V and T are operators that only depend on coordinates and momenta, respectively. For our problem described by Eq. (2), it is straightforward to see that the first two terms on the right hand side of Eq. (2) depend only on position derivatives and thus conveniently define T, while the third term $V = q_1 q_2/R$ is diagonal in position space. Therefore, T and V have diagonal matrix representations in momentum and position space, respectively. Fourier-transforming the wavepacket before and after operating with $e^{-i\Delta tT}$ using a discrete Fourier transform algorithm allows efficient propagation of the wavepacket. The propagation of the wavepacket from t to $t + \Delta t$ is thus given by:

$$\varphi(x,y,t+\Delta t) = e^{-\frac{i\Delta tV}{2}}\mathcal{F}^{-1}\left[e^{-i\Delta tT}\mathcal{F}\left\{e^{-\frac{i\Delta tV}{2}}\varphi(x,y,t)\right\}\right] \tag{5}$$

where $\mathcal{F}$ and $\mathcal{F}^{-1}$ represent forward and backward discrete Fourier transform operations, respectively. In order to calculate them, we employed the FFTW3 [17] library, which gracefully adapts to different parallelizable hardware configurations for efficient calculation.

Our simulations modeled a DT^{2+} field-bound molecule with charges $q_1 = 1$ and $q_2 = 1$ and masses $m_D = 3671.48$ and $m_T = 5497.92$, whose electrons have already been removed by the field ionization pulse before the control pulses are set to begin. At $t = 0$, the nuclear vibrational wavepacket is approximated as a two-dimensional gaussian function:

$$\varphi(x,y) = \frac{1}{\sqrt{\pi\sigma_x\sigma_y}}e^{-\frac{(x-x_0)^2}{2\sigma_x^2} - \frac{(y-y_0)^2}{2\sigma_y^2}} \tag{6}$$

with $\sigma_x = \sigma_y = 0.25$ a.u., and $(x_0, y_0) = (0.0,\ 2.3$ a.u.), somewhat larger than the neutral diatomic molecule bond distance to account for some Coulomb repulsion during the pre-pulse. A Cartesian grid of $2^{14} \times 2^{14}$ points was defined for a 1024 a.u.^{2} area ($\Delta x = \Delta y = 1.953 \cdot 10^{-3}$ a.u.) where Eq. (5) is successively solved until the wavepacket center got to other side of the potential (negative x). When the wavepacket distance to the origin is larger than 2.0 a.u., a time step of 0.1 a.u. was used, and when it is closer, the time step was reduced to 0.001 a.u. to avoid numerical errors.

During its time evolution, the nuclear wavepacket defined by Eq. (6) moves subject to interaction with the repulsive Coulomb potential, and subject to an ultrashort laser pulse that has polarization components along the x and y directions. Both polarizations of the laser electric field were modeled as harmonic carrier waves under a Gaussian envelope:

$$E_x(t) = E_{0x} \cdot e^{-t^2/2\sigma^2} \cdot \cos\left([\omega_0 + \omega_{1x}t]t + \delta_x\right) \tag{7a}$$

$$E_y(t) = E_{0y} \cdot e^{-t^2/2\sigma^2} \cdot \cos\left([\omega_0 + \omega_{1y}t]t + \delta_y\right) \tag{7b}$$

where the half-width $\sigma = 43.8429$ a.u. (5 fs total pulse width) and the carrier frequency $\omega_0 = 0.05695$ a.u. (800 nm wavelength) were equal for both pulses, while the maximum pulse amplitude E_0, linear chirp ω_1 and phase δ were allowed to take different values in the optimization. The vector potentials related to each electric field were integrated from the relationship $E_i(t) = -(1/c)dA_i(t)/dt$, where c is the speed of light, and we neglect the contribution from the electrostatic potential $\varphi(x)$.

In order to compare how well two laser pulses focus the nuclear wavepacket, we defined a square of area $9.5 \cdot 10^{-5}$ a.u.^{2} (25 points) in front of the origin ($x = 0, y = 0$), where the nuclei overlap. At each time step the probability was summed up:

$$P(t) = \sum_{i=1}^{25}|\varphi(x,y)|_i^2\Delta x\Delta y \tag{8}$$

This definition smooths out rapid oscillations in the wavepacket, providing a smooth optimization target. The ratio $P_{\text{optimized}}(t)/P_{\text{un-optimized}}(t)$ approximates the change in fusion yield for s-wave scattering. We will call it the "contact probability."

3. Results

In our calculations, y represents the internuclear axis, while x is the transverse confinement coordinate for the time-propagating nuclear wavepacket. Fig. 1 shows the nuclear wavepacket at $t = 0$ (initial condition), and the same wavepacket after propagation to $t = 167.762$ a.u., when optimal confinement is achieved. This example corresponds to the coherent control field at the top of Table 1. As can be seen, the wavepacket has moved down towards the origin ($x = 0, y = 0$) by about 2 a.u., while remaining confined along the x-axis by the E_x field.

Table 1 summarizes the 9 best control fields discovered during optimization. Fig. 2 shows the best (black) and worst (red) vector potentials, as well as the probabilities $P(t)$ of approaching the neighborhood of ($x = 0$, $y = 0$), as defined in Eq. (8). The original molecular wavefunction has a contact probability $P(0) \approx 10^{-20}$, whereas the best field combination achieves a 16 order of magnitude better contact probability, $P(t)_{\max} \approx 10^{-4}$. The worst/unshaped pulses achieve $P(t)_{\max} \approx 10^{-7}$, so adding coherent control can improve the probability by about 3 orders of magnitude in our 2-D model. The part of the wavepacket around the pixel closest to the origin (around $x = y = 1.953 \cdot 10^{-3}$ a.u.) corresponds to a center-of-mass collision kinetic energy of 13.9 keV. At this energy, the fusion cross section is ~110 mbarn [11], or about 2% of the maximum cross section.

The two simulations in Fig. 2 reach the highest probability $P(t)_{max}$ at different times: the worst simulation at $t \approx 150$ a.u., and the best simulation at $t \approx 167$ a.u. There is a weak trend in Table 1 for better-performing fields building up over longer times (159–165 a.u.), whereas worse performers build up faster (150–158 a.u.). The slower wavepackets tend to spend more time at the origin, rather than shooting past it at $x \neq 0$ and missing the target at a large impact parameter.

Fig. 3 shows the x and y expectation values of the centroid of the nuclear wavepackets from Fig. 2 (same color code). The worst simulation misses the origin by about 1.085 a.u. (0.57 Å), explaining the small value for $P(t)_{max}$. On the other hand, the best simulation drives the wavepacket center to 0.094 a.u. (0.05 Å), more than a

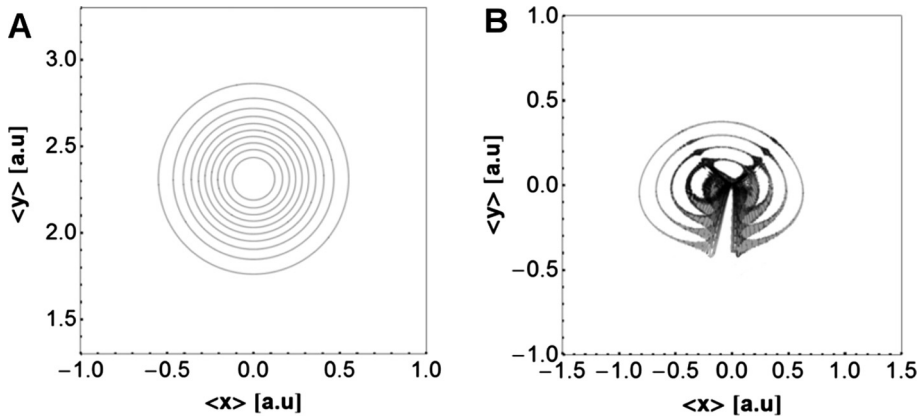

Fig. 1. Panel A and B show the nuclear wavepacket probability contour at t = 0 and t = 167.762 a.u., respectively. Darker contours denote smaller probability. <x> = 0, <y> = 0 marks the location where the nuclei fuse. For time, 1 a.u. = 0.02418 fs. The contours range from ≈0.27 to ≈2.16.

Table 1
Nine best pairs of electric fields, the maximum probability in Eq. (8) reached, and time at which it is reached. All electric fields have $E_0 = 462.166$ a.u., $\sigma = 43.8492$ a.u., $\omega_0 = 0.056938$ (λ = 800 nm). For time, 1 a.u. = 0.02418 fs.

	Electric fields	$P(t)_{max}$	Time (a.u.)
#1	$E_x = \frac{E_0}{4} * e^{-t^2/2\sigma^2} * \cos([\omega_0 - 0.0001t]t)$ $E_y = E_0 * e^{-t^2/2\sigma^2} * \cos([\omega_0]t)$	$3.1 * 10^{-4}$	165.762
#2	$E_x = \frac{E_0}{2} * e^{-t^2/2\sigma^2} * \cos([\omega_0 - 0.0001t]t)$ $E_y = E_0 * e^{-t^2/2\sigma^2} * \cos([\omega_0]t)$	$2.8 * 10^{-4}$	165.721
#3	$E_x = \frac{E_0}{4} * e^{-t^2/2\sigma^2} * \cos([\omega_0]t)$ $E_y = E_0 * e^{-t^2/2\sigma^2} * \cos([\omega_0 - 0.0001t]t + \frac{\pi}{3})$	$2.1 * 10^{-4}$	159.336
#4	$E_x = E_0 * e^{-t^2/2\sigma^2} * \cos([\omega_0 - 0.0001t]t)$ $E_y = E_0 * e^{-t^2/2\sigma^2} * \cos([\omega_0]t)$	$2.0 * 10^{-4}$	165.583
#5	$E_x = \frac{E_0}{2} * e^{-t^2/2\sigma^2} * \cos([\omega_0]t)$ $E_y = E_0 * e^{-t^2/2\sigma^2} * \cos([\omega_0 - 0.0001t]t + \frac{\pi}{3})$	$2.0 * 10^{-4}$	159.186
#6	$E_x = \frac{E_0}{4} * e^{-t^2/2\sigma^2} * \cos([\omega_0]t)$ $E_y = E_0 * e^{-t^2/2\sigma^2} * \cos([\omega_0 + 0.0001t]t)$	$1.6 * 10^{-4}$	152.205
#7	$E_x = E_0 * e^{-t^2/2\sigma^2} * \cos([\omega_0]t)$ $E_y = E_0 * e^{-t^2/2\sigma^2} * \cos([\omega_0 - 0.0001t]t + \frac{\pi}{3})$	$8.0 * 10^{-5}$	158.795
#8	$E_x = \frac{E_0}{2} * e^{-t^2/2\sigma^2} * \cos([\omega_0]t)$ $E_y = E_0 * e^{-t^2/2\sigma^2} * \cos([\omega_0 + 0.0001t]t)$	$5.4 * 10^{-5}$	152.234
#9	$E_x = \frac{E_0}{4} * e^{-t^2/2\sigma^2} * \cos([\omega_0]t)$ $E_y = E_0 * e^{-t^2/2\sigma^2} * \cos([\omega_0]t + \frac{\pi}{3})$	$3.2 * 10^{-5}$	150.237

factor of ten closer. It resembles better a head-on collision, thus peaking at a much higher probability in Fig. 2.

Fig. 4 visualizes the best 20 control fields that were obtained by making use of principal component analysis (PCA) as follows. For the two control field polarizations $E_x(t)$ and $E_y(t)$ in Eq. (7), the five parameters E_{0x}, E_{0y}, ω_{1x}, ω_{1y} and relative phase $\delta_y - \delta_x$ were redefined as

$$\left(\frac{E_{0,x} + E_{0,y}}{2}, \frac{E_{0,x} - E_{0,y}}{2}, \omega_{1,x}, \omega_{1,y}, \delta_y - \delta_x\right) = (a, b, c, d, e). \quad (9)$$

The remaining two parameters σ and ω_0 were kept constant because having a shorter pulse (σ) and a different carrier wave frequency ($\lambda_0 = 2\pi c/\omega_0 \approx 800$ nm) is not possible experimentally. Initially, a genetic algorithm searched the 5-dimensional parameter space of Eq. (9) for the optimal field with a reduced (faster computation) spatial grid size. Then we performed a systematic variation around the optimal values using the final computational grid with a $1.953 \cdot 10^{-3}$ a.u. spacing. To represent visually this 5-dimensional parameter space, we use principal component analysis (PCA) to

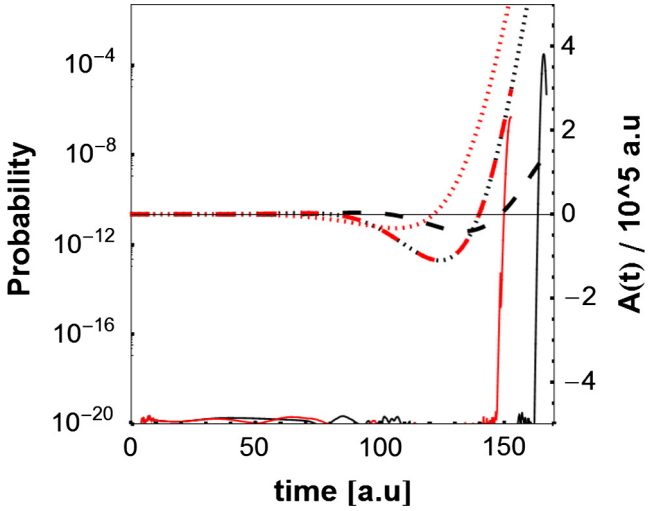

Fig. 2. Probability (solid curves, logarithmic scale) as a function of time for the worst (red) and the best (black) control fields in Table 1. x-axis (long dash) and y-axis (short dash) vector potentials $A(t)$ are also shown. For time, 1 a.u. = 0.02418 fs. (For interpretation of the references to color in this figure legend, the reader is referred to the web version of this article.)

reduce the dimensionality. The three principal components in Fig. 4 explain 97% of the data variability, satisfactorily reducing dimensionality from five parameters (a, b, c, d, e) in Eq. (9) to three principal components, PC1-PC3. They are given by

$$\begin{aligned} \text{PC1} &= -0.674\text{a} + 0.674\text{b} - 0.114\text{c} + 0.196\text{d} - 0.203\text{e} \\ \text{PC2} &= 0.212\text{a} - 0.212\text{b} - 0.466\text{c} + 0.483\text{d} - 0.678\text{e} \\ \text{PC3} &= -0.036\text{a} + 0.036\text{b} - 0.737\text{c} - 0.674\text{d} + 0.0034\text{e} \end{aligned} \quad (10)$$

Darker data points (disks) in Fig. 4 represent larger $P(t)_{\max}$ values, while lighter disks represent smaller $P(t)_{\max}$ values. PC3 provides the single best descriptor for successful control, as can be seen in Fig. 4B, where the 5 best simulations cluster near PC3 = 1. The best $P(t)_{max}$ value is approximately three orders of magnitude larger than the worst (see also the solid red and black curves in Fig. 2).

In Fig. 4A, PCA separates the data into three planes (dashed lines). These planes result from systematically varying the $E_{0,y}/E_{0,x}$ ratio to 1, 2 or 4 (left, middle, and right planes) during the final stage of optimization. A weaker field along the x-axis (transverse direction) relative to the y-axis (collision direction) yields the best control (parameters set "1" in Table 1 and Fig. 4) of the nuclear wavepacket. However, stronger fields in the x-

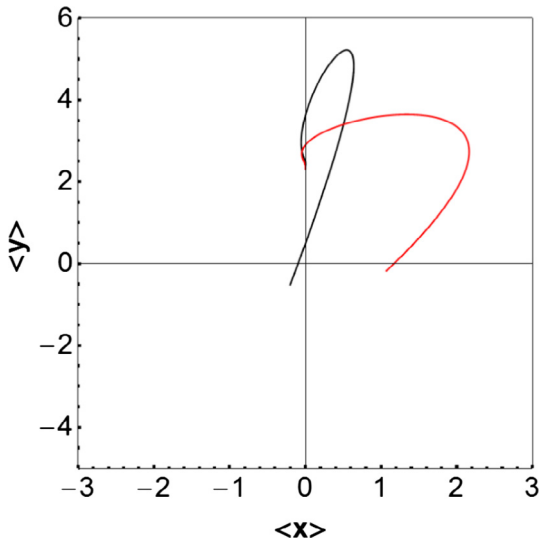

Fig. 3. Nuclear wavepacket centroid expectation values for x and y as a function of time. Black and red represent the best and the worst simulations in Fig. 1. Perfect control would move the centroid to (0,0). (For interpretation of the references to color in this figure legend, the reader is referred to the web version of this article.)

direction, such as parameter set "4" in Fig. 4A, can yield a $P(t)_{max}$ not far below parameter set "1".

A common characteristic of successful control fields is a phase difference, $\delta_y - \delta_x \leq \pi/3$, E_y always having the more positive phase if there is a difference at all. The E_y carrier wave builds up faster as a result (Fig. 2), and confinement along the lateral direction (x-axis) begins later. Cases with a larger difference ($\geq\pi/2$) invariably show a decrease of at least one order of magnitude in $P(t)_{max}$. The dependence on $\omega_{1,x}$ and $\omega_{1,y}$ is quite different (Fig. 4B). Among the best nine cases, not one has a positive chirp $\omega_{1,x}$. The chirp of E_y seems to be less critical.

4. Discussion and conclusion

Our question is whether coherent control of the confinement pulse could further increase the collision probability between two light nuclei. The answer is 'yes.' Our calculations focus on a toy model of the most facile D + T fusion reaction, but $^{11}B + {}^{1}H$ fusion is another interesting candidate for quantum control. This reaction produces only α particles, so it is considered a "clean" fusion process that yields energy without neutron radioactivity. Its disadvantage is that reaching the maximum cross section requires even higher collision energy [12], too far above the kinetic energy we were able to sample with our grid in the 2-D quantum dynamics simulations.

We modeled the fusion enhancement by shaped 5 fs, 800 nm near-infrared pulses that are easily accessible with current laser technology. Pulse-shaped vacuum ultraviolet (VUV) photons with an energy around 20–30 eV are needed to focus the wavepacket to an optimal impact parameter of $2 \cdot 10^{-4}$ Å with the minimal number of photons. Such pulse shaping is currently beyond the state of the art. However, higher energy photons could be an efficient way of compressing the wavepacket further. Indeed, should control with VUV pulses become possible, one can even envision controlling muonic molecules, whose vibrational states have an energy spacing in the 30–100 eV range and lifetimes on the order of picoseconds [18]. Bandrauk and Paramonov have proposed using attosecond VUV pulses to enhance muonic fusion [19]. Adding coherent control to such pulses may be able to push muonic fusion beyond the break-even point for power production, by accelerating the fusion process so that each muon can catalyze more fusion reactions before decaying.

As discussed by Loetstedt et al., proton recollision within molecules could also be used to produce nuclei other than $^{4}He^{2+}$. They performed a classical simulation on $^{15}NH_3$ molecules to produce a field ionized molecule followed by proton recollision with nitrogen. Pulse shaping is likely to enhance the recollision rate in such cases also. Similarly, B_2H_6 could be used as a starting point for boron-hydrogen fusion, rather than diatomic BH or a BH^+ cation beam. Finally, electron impact has been suggested as an analogous scheme for overcoming the Coulombic barrier of colliding nuclei by using a relatively mild electron impact energy source [19].

In summary, we performed quantum wavepacket propagation in a 2-D toy model of two field-bound nuclei in the presence of a time-dependent 800 nm laser pulse that was shaped to exert coherent control over the nuclear wavepacket. The collision probability is enhanced by about 3 orders of magnitude by the best

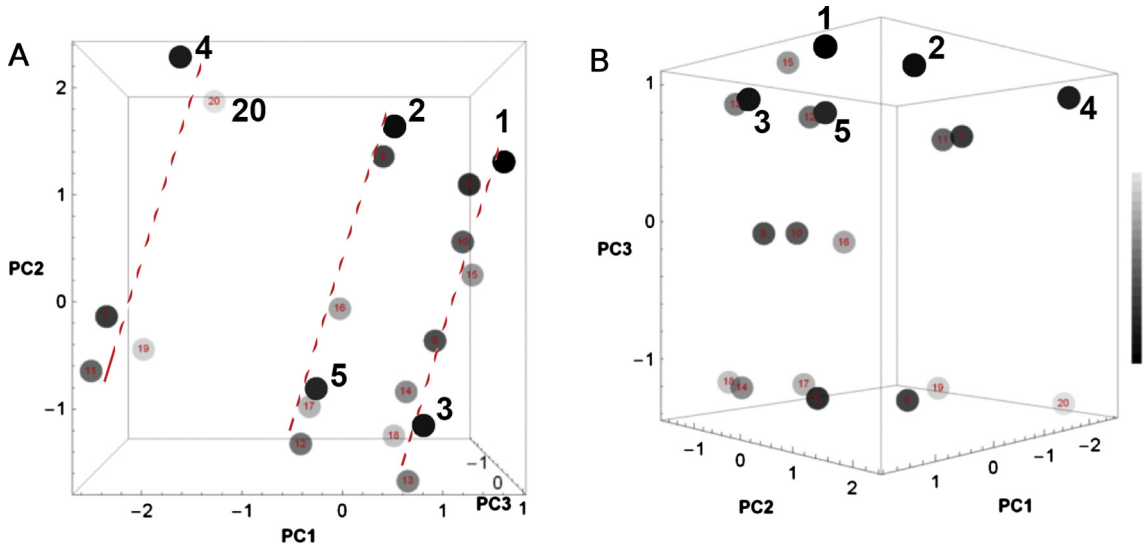

Fig. 4. Principal component analysis of the best 20 simulations. Darker spheres represent better nuclear wavepacket control. The 5 best are labeled. Three planes of points labeled by dashed red lines, containing simulations 4,20 (top plane) and 1,3 (bottom plane) are evident, and due to the discrete ratios of $E_{0,y}/E_{0,x}$ sampled during optimization. (For interpretation of the references to color in this figure legend, the reader is referred to the web version of this article.)

coherent control pulse, and by up to 20 orders of magnitude relative to an electron-bound molecule. Since muonic fusion is already not far from break-even for net energy production, shaped VUV laser pulses, when they become available, could also be an efficient means of enhancing muonic fusion by coherent control.

Acknowledgements

This research was funded by the National Science Foundation grant NSF CHE 1012075. E.B. thanks CONICYT/PAI "concurso nacional apoyo al retorno de investigadores/as desde el extranjero, convocatoria 2013/821320064" for financial support. The authors thank Dmitri Babikov for useful discussions. M.G. thanks the Eiszner family for their generous support via the James R. Eiszner Chair. P.G.W. is grateful for support provided by the D.R. Bullard-Welch Chair at Rice University, Grant C0016.

References

[1] A.M. Dimits, G. Bateman, M.A. Beer, B.I. Cohen, W. Dorland, G.W. Hammett, et al., Comparisons and physics basis of tokamak transport models and turbulence simulations, Phys. Plasmas 7 (2000) 969–983.
[2] S. Nakai, K. Mima, Laser driven inertial fusion energy: present and prospective, Rep. Prog. Phys. 67 (2004) 321–349.
[3] A. Heidenreich, I. Last, J. Jortner, Extreme dynamics and energetics of Coulomb explosion of Xe clusters, Phys. Chem. Chem. Phys. 11 (2009) 111–124.
[4] F. Peano, J.L. Martins, R.A. Fonseca, F. Peinetti, R. Mulas, G. Coppa, et al., Expansion of nanoplasmas and laser-driven nuclear fusion in single exploding clusters, Plasma Phys. Control. Fusion 50 (2008).
[5] M.S. Kushwaha, Observability of the quantum pinch effect in semiconducting quantum wires, Appl. Phys. Lett. 103 (2013) 173116.
[6] D. Mueller, L. Grisham, I. Kaganovich, R.L. Watson, V. Horvat, K.E. Zaharakis, et al., Multiple electron stripping of 3.4 MeV/amu Kr^{7+} and Xe^{11+} in nitrogen, Phys. Plasmas 8 (2001) 1753–1756.
[7] T.C. Wu, C.H. Shi, W.K. An, X. Zhang, X.J. Qiu, Muon motion induced by a superintense laser in muon-catalyzed fusion, Contrib. Plasma Phys. 48 (2008) 307–310.
[8] O. Smirnova, M. Spanner, M. Ivanov, Molecule without electrons: binding bare nuclei with strong laser fields, Phys. Rev. Lett. 90 (2003) 243001.
[9] M. Zhi, A. Sokolov, Numerical study of nuclear collisions induced by superintense ultrashort laser pulses incident on aligned molecules, Phys. Rev. A 80 (2009) 23415.
[10] E. Loetstedt, K. Midorikawa, Nuclear reaction induced by carrier-envelope-phase controlled proton recollision in a laser-driven molecule, Phys. Rev. Lett. 112 (2014).
[11] H.S. Bosch, G.M. Hale, Improved formulas for fusion cross-sections and thermal reactivities, Nucl. Fusion 32 (1992) 611–631.
[12] H. Hora, G.H. Miley, M. Ghoranneviss, B. Malekynia, N. Azizi, X.-T. He, Fusion energy without radioactivity: laser ignition of solid hydrogen-boron (11) fuel, Energy Environ. Sci. 3 (2010) 479–486.
[13] R.S. Craxton, K.S. Anderson, T.R. Boehly, V.N. Goncharov, D.R. Harding, J.P. Knauer, et al., Direct-drive inertial confinement fusion: a review, Phys. Plasmas 22 (2015).
[14] J.D. Jackson, Classical Electrodynamics, Wiley, 1975.
[15] B. Shan, S. Ghimire, Z.H. Chang, Effect of orbital symmetry on high-order harmonic generation from molecules, Phys. Rev. A 69 (2004).
[16] M.D. Feit, J.A. Fleck Jr, A. Steiger, Solution of the Schrödinger equation by a spectral method, J. Comput. Phys. 47 (1982) 412–433.
[17] M. Frigo, S.G. Johnson, The design and implementation of FFTW3, Proc. IEEE 93 (2005) 216–231.
[18] E. Lindroth, J. Wallenius, S. Jonsell, Decay rates of excited muonic molecular ions, Phys. Rev. A 68 (2003).
[19] A.D. Bandrauk, G.K. Paramonov, Excitation of muonic molecules ddμ and dtμ by super-intense attosecond soft X-ray laser pulses: shaped post-laser-pulse muonic oscillations and enhancement of nuclear fusion, Int. J. Mod. Phys. E-Nucl. Phys. 23 (2014).